Available online at www.sciencedirect.com
SCIENCE DIRECT®
Journal of Power Sources 128 (2004) 286–291
JOURNAL OF POWER SOURCES
www.elsevier.com/locate/jpowsour

Short communication

Enhancing the electrochemical properties of LT-$LiCoO_2$ in lithium cells by doping with Mn

A. Caballero [a], L. Hernán [a,*], J. Morales [a], E. Rodríguez Castellón [b], J. Santos [c]

[a] *Departamento de Química Inorgánica e Ingeniería Química, Facultad de Ciencias, Edificio C3, Campus de Rabanales, Universidad de Córdoba, Córdoba 14071, Spain*
[b] *Departamento de Química Inorgánica, Universidad de Málaga, Málaga, Spain*
[c] *Departamento de Química, Universidad de las Islas Baleares, Palma de Mallorca, Spain*

Received 21 February 2003; received in revised form 15 September 2003; accepted 29 September 2003

Abstract

Nearly stoichiometric $LiCo_{1-x}Mn_xO_2$ mixed oxides ($x = 0$, 0.2) were prepared by using a sol–gel method and their electrochemical properties as lithium cell cathodes were examined. Gels of the two samples fired at 400 °C exhibited the same structure as LT-$LiCoO_2$, with the transition elements in a tervalent state as revealed by XPS spectroscopy. A modified spinel structure model is proposed to account for the X-ray diffraction data. Substitution of Co by Mn ions has the following favorable effects on the electrochemical properties: (i) a decrease in polarization between the charge and discharge curves; (ii) an increase in capacity delivered by the cell; (iii) a marked improvement in the cycling properties of the cell, particularly when the calcining temperature is raised to 600 °C. The enhanced cell performance is ascribed to lithium occupying in an orderly manner available positions in the modified spinel structure adopted. The presence of Mn enhances cation ordering, thus increasing the reversibility of the lithium reaction.
© 2003 Elsevier B.V. All rights reserved.

Keywords: Lithium batteries; Lithium–cobalt–manganese oxides

1. Introduction

$LiCoO_2$ has been commercially available for manufacturing Li-ion batteries since the early 1990s [1]. This compound exhibits two different phases that have been extensively studied, viz. a low-temperature phase (LT-$LiCoO_2$) [2–6] and one that is stable at high temperatures (HT-$LiCoO_2$) [7–10]. Only the HT phase synthesized above 800 °C possesses good electrochemical properties; its industrial preparation, however, involves high costs. Unfortunately, the more affordable alternative (LT-$LiCoO_2$) fails to maintain cell performance over the first few cycles. One procedure that often provides an improved electrochemical response from Li-containing transition metal oxides in lithium cells involves replacing part of the base transition metal by another element. This methodology has been extensively applied to HT-$LiCoO_2$, where Co has been substituted by different elements such as Ni [11,12], Mn [13,14], Fe [15,16], Cr [17], Rh [18], Al [19,20], Mg [21] with varying success. The conventional ceramic method is commonly used to accomplish these substitution reactions. By contrast, few studies on LT-$LiCo_{1-x}M_xO_2$, have been conducted, probably because of the difficulty in finding appropriate conditions for the synthesis of these metastable phases. The beneficial effect of Co substitution in LT-$LiCoO_2$ was demonstrated by Gummow and Thackeray [22] in the LT-$LiCo_{0.9}Ni_{0.1}O_2$ phase; however, effectively enhancing its electrochemical performance required an acid pretreatment.

In this work, LT-$LiCo_{1-x}Mn_xO_2$ ($x = 0$, 0.2) phases were prepared by using a sol–gel method and further calcination of the gel at a relatively low-temperature (400 °C). A comparison of the electrochemical properties of these systems revealed the favorable effect of Mn on the capacity and cycling properties of the cell, particularly as regards $LiCo_{0.8}Mn_{0.2}O_2$.

2. Experimental

LT-$LiCo_{1-x}Mn_xO_2$ phases ($x = 0$, 0.2) were synthesized by using sol–gel method based on the reaction between $Co(acac)_3$ (acac = acetylacetonate) and Li_2CO_3 in boiling propionic acid under vigorous stirring, and subsequently adding $Mn(acac)_3$ to obtain the doped forms. Co

* Corresponding author. Tel.: +34-957-218620; fax: +34-957-218621.
E-mail address: iq1hepal@uco.es (L. Hernán).

0378-7753/$ – see front matter © 2003 Elsevier B.V. All rights reserved.
doi:10.1016/j.jpowsour.2003.09.061

and Mn acetylcetonates were prepared by following conventional procedures [23] and the sol–gel procedure is described in detail elsewhere [24].

X-ray powder diffraction (XRD) patterns were recorded on a Siemens D5000 diffractometer, using Cu $K\alpha_{1,2}$ radiation and a graphite monochromator. The scanning conditions were 15–110° (2θ), a 0.03° (2θ) step and 15 s per step. X-ray photoelectron spectra (XPS) were obtained on a Physical Electronics PHI 5700 spectrometer using unmonochromated Mg Kα radiation (1253.6 eV) as excitation source. Charge referencing was done against adventitious hydrocarbon (C 1s 284.8 eV).

Electrochemical measurements were carried out in two-electrode cells, using Li (supplied by Strem) as anode. Powdered pellets 7 mm in diameter were prepared by pressing, in a stainless steel grid, ca. 10 mg of active material with graphite (7.5 wt.%), acetylene black (7.5 wt.%) and PTFE (5 wt.%). The electrolyte, supplied by Merck, was 1 M anhydrous $LiPF_6$ in a 1:2 mixture of ethylene carbonate and diethyl carbonate. Cells were assembled in an M-Braun glove-box. Cyclic voltammetry tests were performed with a Solartron 1286 Electrochemical Interface controlled via the CorrWare and CorrView software packages as run on a PC 486 computer. Curves were recorded at a scan rate of 50 μV/s. Cycling tests were performed under a galvanostatic regime on a McPile II potentiostat–galvanostat system.

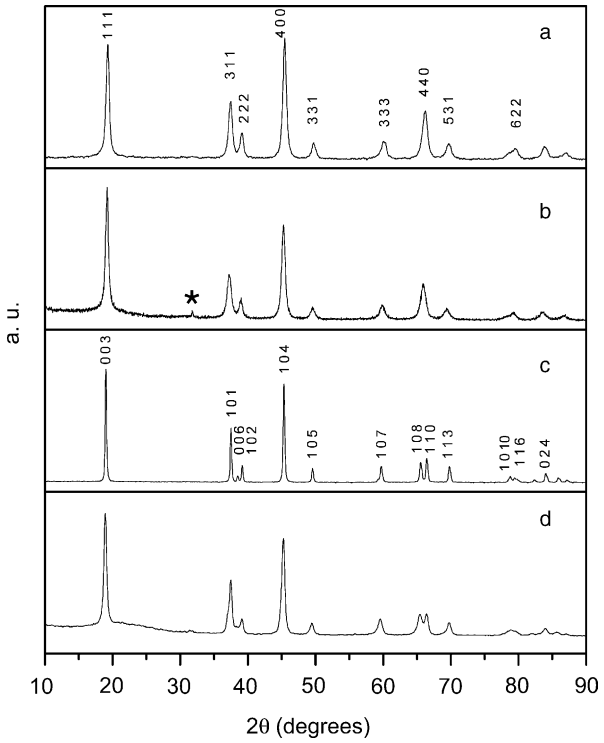

Fig. 1. X-ray diffraction patterns for the gel calcined at 400 °C (a and b) and 600 °C (c and d). Compositions: $LiCoO_2$ (a and c); $LiCo_{0.8}Mn_{0.2}O_2$ (b and d) (asterisk denotes Li_2CO_3).

3. Results and discussion

Fig. 1a and b shows the XRD patterns obtained after heating the gels at 400 °C for 24 h, followed by manual grinding and recalcining at 400 °C for another 24 h (hereafter LT samples). Both patterns coincide with that of LT-$LiCoO_2$ [2,3] and can be indexed in the hexagonal system. An additional, very weak peak at ca. 2.810 Å is observed for the Mn-containing samples. Ascribing this reflection to the (2 2 0) peak of the Co_3O_4 spinel is rather speculative as the stronger peaks for this phase are absent. The fact that it coincides with the strongest peak for Li_2CO_3 and virtually disappears as the temperature is raised justifies its assignation to unreacted traces of this salt. Weight loss data revealed the content in the salt to be below 5%. Substitution of Co by Mn, was found to result in slight expansion of the unit cell parameters consistent with the differences in size between Co^{3+} and Mn^{3+} (with an ionic radius of 0.68 and 0.78 Å, respectively) (Table 1). The *c*/*a* ratio tends to decrease slightly with increasing Mn content and approaches 4.90 (the value provided by an ideally cubic-close-packed structure). Thus, the XRD patterns in Fig. 1a and b can also be indexed in a face-centered cubic unit cell (Fd3m). In fact, some authors regard LT-$LiCoO_2$ as an intermediate between a layered structure (R3m space group, $(Li)_{3a}\{Co\}_{3b}O_2$ configuration) and a spinel-type structure (Fd3m space group, with cations occupying octahedral positions in an $(Li_2)_{16c}\{Co_2\}_{16d}O_4$ configuration) [25].

Further heating at 600 °C for 24 h caused structural distortion that decreased the unit cell symmetry and resulted in subsequent splitting of some spinel peaks. For LT-$LiCoO_2$ (Fig. 1c), the spinel (2 2 2) splits into the hexagonal (0 0 6) and (0 1 2) peaks; also, the spinel (4 4 0) peak splits into the hexagonal (1 0 8) and (1 1 0) peaks. These results, together with a *c*/*a* ratio ≈5 (Table 1) and the appreciably decreased peak broadening, are consistent with a high cation ordering in the hexagonal structure despite the relatively low synthesis temperature used. In fact, the pattern is similar to that

Table 1
Lattice constants for samples fired at different temperatures

Sample	400 °C				600 °C		
	a	*c*	*c*/*a*	*a* (Fd3m)	*a*	*c*	*c*/*a*
$LiCoO_2$	2.818	13.871	4.922	7.979 (5)	2.806	14.022	4.99
$LiCo_{0.8}Mn_{0.2}O_2$	2.830	13.896	4.910	8.009 (6)	2.812	14.074	5.00

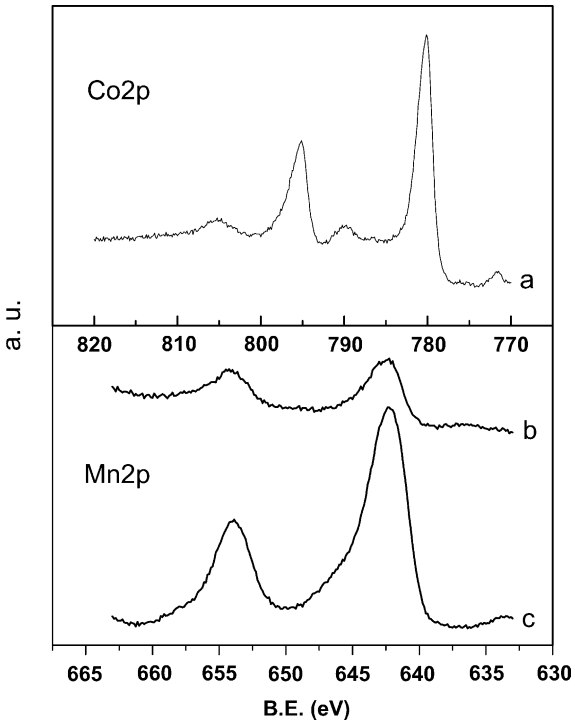

Fig. 2. XPS spectra for $LiCoO_2$ (a), $LiCo_{0.8}Mn_{0.2}O_2$ (b) and $Mn(CH_3–COO)_3{\cdot}2H_2O$ (c).

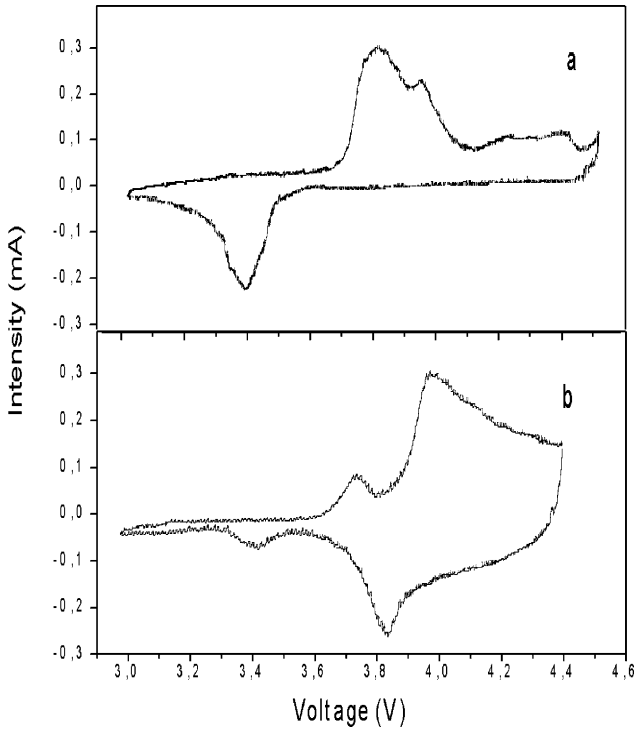

Fig. 3. Cyclic voltammograms for LT-$LiCoO_2$ (a) and LT-$LiCo_{0.8}Mn_{0.2}O_2$ (b).

for HT-$LiCoO_2$ synthesized at 800 °C using the conventional ceramic method [7]. The Mn-containing sample behaves somewhat differently. Thus, the small peak at 2.810 Å tends to disappear at 600 °C through thermal decomposition of carbonate impurities, and only the spinel (4 4 0) peak is clearly split (see Fig. 1d). Moreover, the peaks are broader than those for the undoped oxide, which suggests that Mn slows down hexagonal distortion and that a calcination temperature as high as 700 °C is required to detect splitting of the two spinel peaks.

The Co 2p spectrum (Fig. 2a) exhibits two well-defined peaks centered at 780.1 and 795.1 eV, that correspond to $2p_{3/2}$ and $2p_{1/2}$ photoemission peaks, respectively. A satellite peak is also clearly observed at 789.8 eV. The binding energy and the profile shape are typical of Co^{3+}, probably in a low-spin state [26]. The main component of the Mn 2p spectrum (Fig. 2b) is centered at 642.3 eV and lacks the strong satellite structures typical of Mn^{2+} compounds [27]. However, the fact that this value is closer to that for MnO_2 (642.4 eV) [28] than to that for Mn_2O_3 (641.6 eV) [29] adds some uncertainty to the valence state of this element. In order to shed light on this problem, the spectrum for commercially available $Mn(CH_3–COO)_3{\cdot}2H_2O$ was recorded for comparison. The choice of a salt was based on the reduced non-stoichiometry of salts relative to oxides. The Mn 2p spectrum shown in Fig. 2c has the same features and a $2p_{3/2}$ binding energy of 642.3 eV, which is similar to that found for the ternary oxide. Based on these results, we believe that Mn is present as Mn^{3+}, even though we are aware of the limitations of this spectroscopic method derived from its ability to analyze only a few nanometers in depth, and of the fact that Mn^{3+} is an unstable oxidation state towards disproportion into Mn^{4+} and Mn^{2+}. However, the absence of satellites in the Mn 2p photoemission peak, which rules out the presence of Mn^{2+}, provides additional evidence that no such reaction takes place and that the tervalent oxidation state can be maintained. Finally, the Mn/Co ratio obtained from the XPS, 0.25, is in excellent agreement with that obtained from the precursor content ratio. This can be taken as indirect evidence of homogeneous distribution of both elements in the bulk.

Fig. 3 compares the cyclic voltammograms for LT-$LiCoO_2$ and LT-$LiCo_{0-8}Mn_{0.2}O_2$ electrodes recorded against a pure lithium anode. Notwithstanding the structural similarity, there are some differences resulting from those in composition. Thus, the CV shape for LT-$LiCoO_2$ is similar to that reported by Gummow et al. [30], but the two-step process for lithium extraction is better resolved probably due to the different experimental set-up. The anodic curve exhibits two peaks at 3.81 and 3.95 V, whereas the cathodic wave exhibits only one, rather asymmetric peak at 3.39 V. This, together with the significant separation between both signals, is indicative of low reversibility in the lithium reaction. The CV shape for $LiCo_{0.8}Mn_{0.2}O_2$ is different from that reported by Waki et al. [31] for a compound of similar composition but prepared at 700 °C in an oxygen atmosphere; no peak-shaped CV was observed, probably because of the high scan rate used (1 mV/s). In our case, the anodic scan ex-

hibits two peaks at 3.75 and 3.97 V; the reduction curve has two better-defined peaks at 3.85 and 3.42 V, and the distance between the strong anodic and cathodic peaks is only 0.12 V (compared with ca. 0.4 V in the undoped sample). In addition to some shifts in the potential values of the peaks, intensities are reversed with respect to LT-$LiCoO_2$. The presence of Mn significantly decreases the intensity of the low-voltage peak and increases that of the high-voltage peak. The modified spinel structure can afford a plausible model to the CV shape. The ideal configuration, $(Li_2)_{16c}[Co_2]_{16d}O_4$ should exhibit a single peak in the cyclic voltammograms, as all lithium ions would occupy equivalent positions. The finding of two peaks for the oxidation process might reveal that lithium ions occupy two different positions (viz. 16c and 16d octahedral sites) and shift some cobalt ions to 16c sites. This disorder can also be inferred from the X-ray pattern of Fig. 1a—note the similarity in intensity of the (1 1 1) and (4 0 0) peaks ($I_{111}/I_{400} = 0.93$). In fact, the stronger peak in the voltammogram is that appearing at the lower voltage and associated with lithium removal from 16d (the more unfavorable position). The presence of Mn significantly decreases this peak and increases the high-potential peak, thereby reflecting the occupancy of the 16d positions by transition ions, and the presence of an increased proportion of lithium ions at 16c positions. This increased ordering in Li, Mn and Co cations is also apparent from the X-ray patterns for the Mn-containing samples (Fig. 1b and c), where the $I_{(111)}/I_{(400)}$ is significantly higher ($I_{111}/I_{400} = 1.27$). A higher intensity for the (1 1 1) reflection compared to the (4 0 0) reflection is indicative of an improvement in cation ordering [32]. One question that arises from these data is why the presence of Mn delays splitting of the spinel peaks and the adoption of the hexagonal-symmetry highly ordered (e.g. R3m). One plausible explanation may be the strong tendency of the Li–Mn–O system to adopt a three-dimensional framework. In fact, layered $LiMnO_2$ cannot be synthesized directly and requires an alternative method such as ion-exchange of layered $NaMnO_2$ [33]. Moreover, the strong Jahn-Teller distortion, typical of Mn^{3+} ions in a high-spin configuration, may hinder the ion migrations required to reach the ideal layered structure.

Fig. 4 shows the voltage profiles for the second charge and discharge as recorded in the galvanostatic mode between 2.0 and 4.5 V, using a current density of 0.250 mA/cm^2. Under these conditions, LT-$LiCo_{0.8}Mn_{0.2}O_2$ provides the best electrochemical response. One can remove as much as 0.6 Li^+ per unit formula compared with LT-$LiCoO_2$ (ca. 0.4 Li^+). Also, its discharge curve possesses the lowest polarization, particularly up to 3.5 V. Fig. 5 shows the delivered cathode capacity for different cycles. The increased capacity exhibited by the LT-$LiCo_{0.8}Mn_{0.2}O_2$ sample in the first cycle is retained on further cycling. Even though the capacity of the electrodes fades on cycling, LT-$LiCoO_2$ exhibits a steeper decline in the first cycles. Such poor

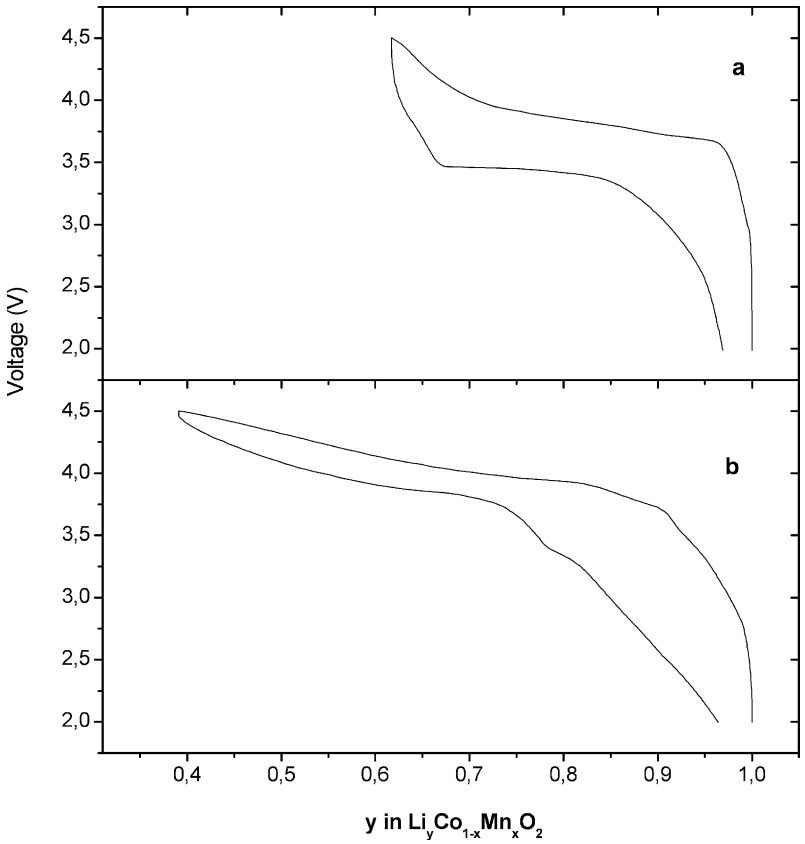

Fig. 4. Second charge and discharge curve for LT-$LiCoO_2$ (a) and LT-$LiCo_{0.8}Mn_{0.2}O_2$ (b).

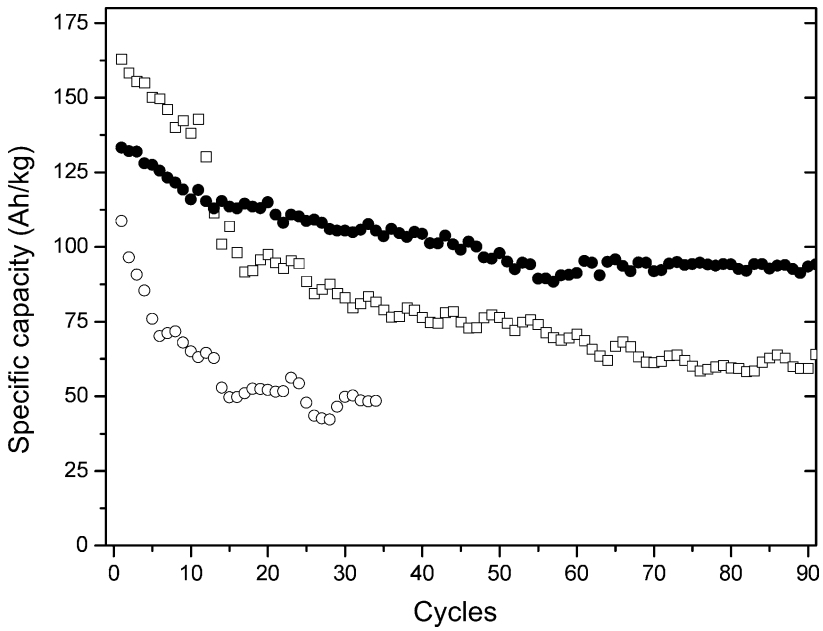

Fig. 5. Capacity delivered by the cell vs. number of cycles for LT-$LiCoO_2$ (○), LT-$LiCo_{0.8}Mn_{0.2}O_2$ (□) and $LiCo_{0.8}Mn_{0.2}O_2$ heated at 600 °C (●).

electrochemical performance is typical of this compound and has been ascribed to the presence of some cobalt ions at octahedral 16c sites. The experimental data discussed above are consistent with this explanation. The substitution of Co by Mn reduces the occupancy of 16c sites by multivalent atoms and improves the electrochemical performance of LT-$LiCo_{0.8}Mn_{0.2}O_2$. The improved electrochemical response of LT-$LiCo_{0.8}Mn_{0.2}O_2$ is consistent with the apparent chemical diffusion coefficients measured by Waki et al. [31] in single microparticles by using the microelectrode technique. The value for HT-$LiCoO_2$ was doubled when Co was substituted by Mn (which increases the kinetic reversibility of the lithium insertion/de-insertion reaction).

Earlier work with this synthesis procedure revealed that a low calcining temperature for the gel (e.g. 400 °C) resulted in a poor electrochemical response of the material acting as electrode in lithium cells [34]. A moderate increase in the calcining temperature (e.g. 600 °C) resulted in improved electrode performance. Increased crystallinity and changes in particle shape have been proposed to explain these results. Based on these previous findings, at this preliminary stage we studied the cycling properties of $LiCo_{0.8}Mn_{0.2}O_2$ (the sample with the better electrochemical properties) heated at 600 °C for 24 h. Although the initial capacity of the cell made from this sample was 135 A h/kg, which is ca. 14% lower than that for the sample heated at 400 °C, this superiority vanished after the 15th cycle (see Fig. 5). Beyond that point, the delivered capacity slowly faded on cycling and fell to a constant value of 100 A h/kg in the potential window 4.5–2.00 V. These properties make this low-temperature mixed oxide an attractive cathode material that can be matched with HT-$LiCoO_2$ once doping metal content, phase purity, particle size and morphology have been optimized.

4. Conclusions

A sol–gel method that starts from tervalent acetylacetonates and uses propionic acid as the resin framework was found to be effective for preparing low-temperature Mn-doped $LiCoO_2$ oxides based on the LT-$LiCoO_2$ system. This undoped material exhibits a poor electrochemical performance as cathode in lithium cells that is substantially improved by the presence of Mn in its structure. Thus, a cell working with $LiCo_{0.8}Mn_{0.2}O_2$ obtained at a moderate calcining temperatures (ca. 600 °C) retains good cycling properties over a large number of cycles and delivers quite an acceptable capacity. A model based on the shifts in cation distribution induced by the substitution of Co by Mn is proposed to account for the improved reversibility of the lithium insertion/de-insertion reaction.

Acknowledgements

The authors gratefully acknowledge financial support from MCYT (Project MAT2002-04477-C02-02) and Junta de Andalucía (Group FQM 0175).

References

[1] T. Nagura, in: Fourth International Rechargeable Battery Seminar, Deerfield Beach, FL, 1990.

[2] R.J. Gummow, M.M. Thackeray, W.I.F. David, S. Hull, Mater. Res. Bull. 27 (1992) 327.
[3] M. Antaya, K. Cearns, J.S. Preston, J.N. Reimers, J.R. Dahn, J. Appl. Phys. 76 (1994) 2779.
[4] D. Larcher, M.R. Palacín, G.G. Amatucci, J.M. Tarascon, J. Electrochem. Soc. 144 (1997) 408.
[5] J. Kim, P. Fulmer, A. Manthiram, Mater. Res. Bull. 34 (1999) 571.
[6] O.A. Brylev, O.A. Shlyakhtin, T.L. Kulova, A.M. Skundin, Yu.D. Tretyakov, Solid State Ionics 156 (2003) 291.
[7] K. Mizhshima, P.C. Jones, P.J. Wiseman, J.B. Goodenough, Mater. Res. Bull. 15 (1980) 783.
[8] J.N. Reimers, J.R. Dahn, J. Electrochem. Soc. 139 (1992) 2091.
[9] M. Yoshio, H. Tanaka, K. Tominaga, H. Noguchi, J. Power Sources 40 (1992) 347.
[10] G.G. Amatucci, J.M. Tarascon, L.C. Klein, J. Electrochem. Soc. 143 (1996) 1114.
[11] T. Ohzuku, A. Ueda, J. Electrochem. Soc. 144 (1997) 2780.
[12] C. Delmas, M. Menetrier, L. Croguennec, I. Saadoune, A. Roegier, C. Poouillerie, G. Prado, M. Grune, L. Fournes, Electrochim. Acta 45 (1999) 243.
[13] R. Stoyanova, E. Zhecheva, L. Zarkova, Solid State Ionics 73 (1994) 233.
[14] A.R. Armstrong, A.D. Robertson, R. Gitzendanner, P.G. Bruce, J. Solid State Chem. 145 (1999) 549.
[15] M. Holzapfel, R. Schreiner, A. Ott, Electrochim. Acta 46 (2001) 1063.
[16] H. Kobayashi, H. Shigemura, M. Tabuchi, H. Sakaebe, K. Ado, H. Kageyama, A. Hirano, R. Kanno, M. Wakita, S. Morimoto, S. Nasu, J. Electrochem. Soc. 147 (2000) 960.
[17] S. Madhavi, G.V. Subba Rao, B.V.R. Chowdari, S.F.Y. Li, Electrochim. Acta 48 (2002) 219.
[18] S. Madhavi, G.V. Subba Rao, B.V.R. Chowdari, S.F.Y. Li, J. Electrochem. Soc. 148 (2001) 1279.
[19] G. Ceder, Y.M. Chiang, D.R. Sadoway, M.K. Aydinol, Y.I. Jang, B. Huang, Nature 392 (1998) 694.
[20] W. Yoon, K.K. Lee, K.B. Kim, J. Electrochem. Soc. 147 (2000) 2023.
[21] H. Tukamoto, A.R. West, J. Electrochem. Soc. 144 (1997) 3164.
[22] R.J. Gummow, M.M. Thackeray, J. Electrochem. Soc. 140 (1993) 3365.
[23] J.D. Woollins (Ed.), Inorganic Experiments, VCH Publishers, New York, 1994, p. 116.
[24] L. Hernán, J. Morales, L. Sánchez, J. Santos, E. Rodríguez Castellón, Solid State Ionics 133 (2000) 179.
[25] Y. Shao-Horn, S.A. Hackey, A.J. Kahain, M.M. Tackeray, J. Solid State Chem. 168 (2002) 60.
[26] J.C. Dupin, D. Gonbeau, I. Martin-Litas, P. Vinatier, A. Levasseur, J. Electron. Spectrosc. Relat. Phenom. 120 (2001) 55.
[27] A.E. Bocquet, T. Mizokawa, T. Saito, H. Namatame, A. Fujimori, Phys. Rev. B 42 (1992) 3777.
[28] C.D. Wagner, W.M. Riggs, L.E. Davis, J.F. Moulder, G.E. Mullenberg, in: Handbook of X-Ray Photoelectron Spectroscopy, Perkin-Elmer Corporation, Physical Electronics Division, Eden Pairie, MN, 1979.
[29] D. Briggs, M.P. Seach, in: Practical Surface Analysis, vol. 1, Wiley, New York, 1990, p. 598.
[30] R.J. Gummow, M.M. Tackeray, W.I.F. David, S. Hull, Mater. Res. Bull. 27 (1992) 327.
[31] S. Waki, K. Dokka, T. Itoh, M. Nishizawa, T. Abe, I. Uchida, J. Solid State Electrochem. 4 (2000) 205.
[32] R. Gupta, A. Manthiram, J. Solid State Chem. 121 (1996) 483.
[33] A.R. Amstrong, P.G. Bruce, Nature 61 (1996) 309.
[34] L. Hernán, J. Morales, L. Sánchez, J. Santos, Solid State Ionics 104 (1997) 205.